ACS OMEGA

http://pubs.acs.org/journal/acsodf

Article

Ionic Liquid (1-Ethyl-3-methylimidazolium Acetate) Plasticization of Chitosan-Based Bionanocomposites

Pei Chen, Fengwei Xie,* Fengzai Tang, and Tony McNally*

Cite This: https://dx.doi.org/10.1021/acsomega.0c02418

Read Online

ACCESS | Metrics & More | Article Recommendations | Supporting Information

ABSTRACT: The structure and properties of different biopolymer composites based on chitosan and chitosan/carboxymethyl cellulose (CMC) are governed by multiple structure−property relationships associated with different phase interactions. Plasticization of these matrices with ionic liquid 1-ethyl-3-methylimidazolium acetate ([C_2mim][OAc]) played a dominant role, increasing the mobility of biopolymer chains as well as ions and associated dipoles but reducing biopolymer chain interactions, crystallinity, and thermal stability. These structural changes led to higher matrix ionic conductivity, shorter electrical relaxation time, and greater matrix ductility. The inclusion of graphene oxide (GO) and reduced GO (rGO) also influenced the structure and properties of these bionanocomposites by disrupting the biopolymer hydrogen bonding and/or polyelectrolyte complexation (PEC) and interacting with [C_2mim][OAc]. The impact of GO/rGO was more evident for 20 wt % [C_2mim][OAc], such as increased crystallinity and thermal stability of chitosan. PEC was hindered with excess (40 wt %) [C_2mim][OAc] added and further hindered again when rGO was included. This study shows that the structure and properties of bionanocomposites are not just determined by the surface chemistry of GO/rGO but can also be influenced by multiple interactions involving plasticizers such as ILs and additional biopolymers.

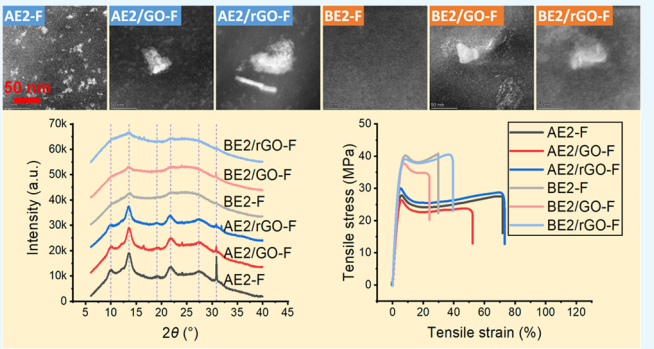

INTRODUCTION

Biopolymers, which are defined as macromolecules (including proteins, nucleic acids, and polysaccharides) formed by living organisms according to the IUPAC, have attracted much interest in materials development in recent years due to their renewability, biodegradability, and inherent functionality (*e.g.*, antimicrobial activity of chitosan). Polymer chain interactions such as hydrogen bonding play a pivotal role in determining the structure and properties of biopolymers. A high degree of hydrogen bonding between biopolymer chains may realize drastically improved mechanical properties.[1−3] Nonetheless, to assist in the processing of biopolymers and to fabricate biopolymers with increased ductility, plasticizers need to be introduced to the biopolymer formulation, which can disrupt the intrinsic hydrogen-bonding network, control the density of newly formed hydrogen bonds, and increase chain mobility, thus modifying material properties. For this purpose, ionic liquids (ILs), often referred to as "green solvents", have recently attracted great interest for processing and plasticization of biopolymers.[4−12] ILs that contain a strongly basic, hydrogen-bond-accepting anion (*e.g.*, carboxylates or halides) are capable of disrupting the intermolecular hydrogen bonding wholly or partially in biopolymer networks.[12] Moreover, the use of ILs could lead to the development of advanced biopolymer materials such as ionically conducting polymers or solid polymer electrolytes.[13−20]

In this work, we investigated the effect of an IL, 1-ethyl-3-methylimidazolium acetate ([C_2mim][OAc]), added at 20 or 40 wt % levels, on the structure and properties of different chitosan and chitosan/carboxymethyl cellulose (CMC) composites. [C_2mim][OAc] has desirable properties such as low melting point (<−20 °C), viscosity (10 mPa·s at 80 °C), toxicity (LD_{50} > 2000 mg·kg^{-1}), corrosiveness, and adequate biodegradability,[21] which make this IL suitable for processing of biopolymers with minimal impact on health and the environment.

In composites, the chitosan polycation and the CMC polyanion are expected to participate in polyelectrolyte complexation (PEC) through electrostatic attraction as a type of dynamic bonding. The advantages of PEC have been recently demonstrated in the development of various advanced biopolymer materials with superior properties to that any single biopolymer can achieve, such as mechanical[22−24] and

Received: May 22, 2020
Accepted: July 8, 2020

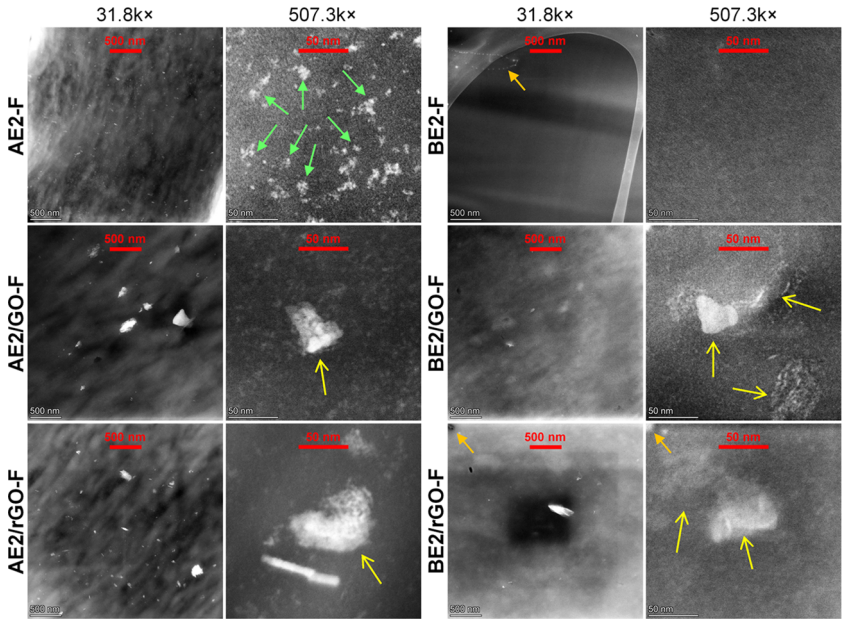

Figure 1. Scanning transmission electron microscopy high-angle annular dark-field imaging (STEM-HAADF) images of the different biopolymer and bionanocomposite films. The green arrows indicate nondispersed particulate features (chitosan structure); the yellow arrows indicate large flocculent substances (GO or rGO nanosheets not fully exfoliated); the dotted features at the top left of the images (examples indicated by the orange arrows) were STEM beam-induced damages.

barrier properties,[25] hydrolytic stability,[26] and cell adhesiveness.[27]

The nanofillers used, graphene oxide (GO) and reduced graphene oxide (rGO), have different concentrations of oxygen-containing groups (*e.g.*, −COOH and −OH) and negative charges[28] and, thus, should have different degrees of hydrogen-bonding and electrostatic interactions with biopolymers. Graphene has drawn great attention due to its exceptional thermal conductivity, mechanical properties, and electronic transport properties.[29] Moreover, two-dimensional (2D) graphenic nanomaterials have also demonstrated antimicrobial activity.[30−33] Thus, the incorporation of GO and rGO into biopolymer matrices (resulting in bionanocomposites) is expected to enhance the properties and functionality of the biopolymers for possible wider application.

In this research, effective mixing of the different components (*i.e.*, chitosan, CMC, GO/rGO, and ILs) was achieved by thermomechanical kneading of the condensed material systems at high viscosity. We hypothesize that the structure and properties of the dual bionanocomposites are not wholly determined by the surface chemistry of the 2D carbon nanomaterial. How [C_2mim][OAc] influences hydrogen-bonding and electrostatic interactions among the different components and, subsequently, the structure and properties of the resulting composites have not been widely reported before.

RESULTS AND DISCUSSION

Morphology. Figure 1 shows the nanoscale structures of the different formulations examined by scanning transmission electron microscopy (STEM). All of the chitosan-based (A) samples at a high magnification (507k×) showed some particulate features, possibly associated with chitosan structures not destroyed by processing or the formation of new crystals (further discussed in XRD results). AE2/GO-F and AE2/rGO-F (the chitosan matrix plasticized by 20 wt % [C_2mim][OAc] and included with GO or rGO) displayed additional larger features, most probably agglomerations of GO/rGO. As these agglomerates were small in number and scattered very sparsely, it was likely that more finely dispersed, few-layer GO/rGO nanosheets were also present but were not readily visible under STEM. In contrast, BE2-F (the chitosan/CMC matrix plasticized by 20 wt % [C_2mim][OAc] without nanofiller) exhibited a clear morphology without particulate features seen for the A-samples. In comparison, the STEM images of BE2/GO-F and BE2/rGO-F (the chitosan/CMC matrix plasticized by 20 wt % [C_2mim][OAc] and included with GO or rGO) only showed some flocculent substances clearly observable at a high magnification (507k×), indicating the presence of GO or rGO.

The oxygen-containing groups (*e.g.*, −COOH and −OH) and negative charges resulting from ionization of carboxylic acid and phenolic hydroxyl groups on the GO nanosheets can interact effectively with the chitosan polycation through hydrogen bonding and electrostatic attraction.[28] Moreover, different studies[28,34,35] have shown the excellent dispersion of GO in chitosan materials. Here, our STEM images indicated similar morphologies for the samples containing GO and rGO, irrespective of matrix type, demonstrating the efficient dispersion of GO/rGO in both matrices enabled by thermomechanical mixing.

Crystalline Structure. Figure 2 shows the X-ray diffraction (XRD) curves for the different films. As discussed previously,[26] these processed samples should contain predominantly a recrystallized structure, with their XRD patterns entirely different from that for unprocessed chitosan. With 40 wt % [C_2mim][OAc], the peak intensities (especially the one at 13.6°) were moderately reduced, indicating that a higher IL content may have hindered chitosan recrystallization. Moreover, for the A-matrix containing either 20 or 40 wt % [C_2mim][OAc], addition of rGO led to less intense XRD peaks, indicating rGO might have suppressed chitosan recrystallization. However, no such effect was apparent for

https://dx.doi.org/10.1021/acsomega.0c02418
ACS Omega XXXX, XXX, XXX−XXX

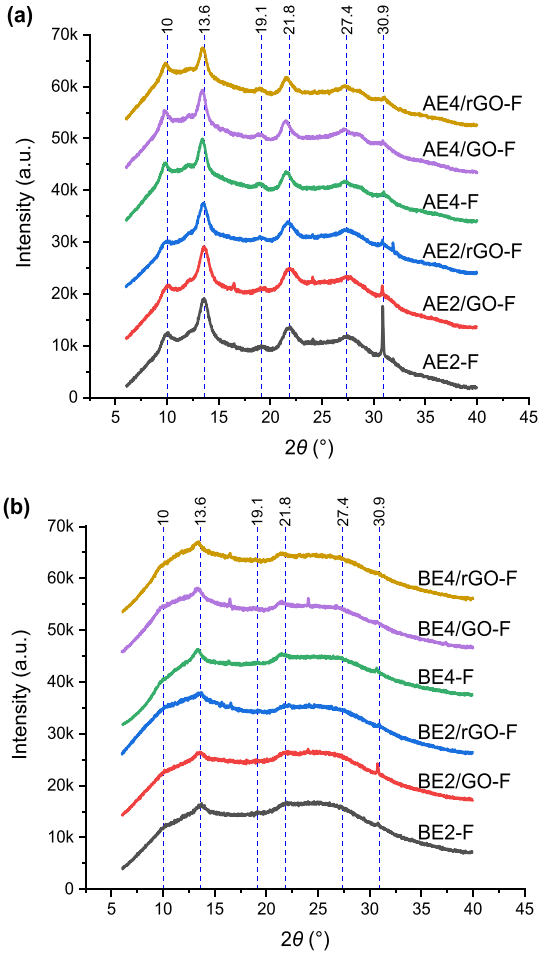

Figure 2. X-ray diffractograms for the different biopolymer and bionanocomposite films: (a) chitosan matrix and (b) chitosan/CMC matrix. The reference lines indicate characteristic peaks for AE2-F.

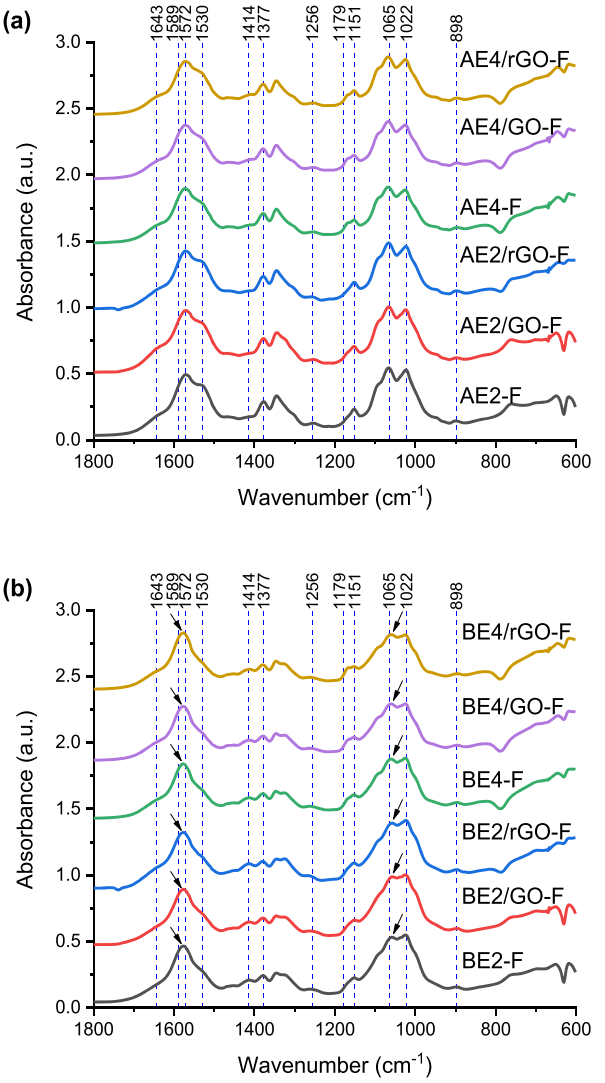

Figure 3. FTIR spectra of the different biopolymer and bionanocomposite films: (a) chitosan matrix; (b) chitosan/CMC matrix. The reference lines indicate characteristic bands for unprocessed CMC (1589, 1414, and 1022 cm^{-1}),[26] unprocessed chitosan (1643, 1572, 1530, 1377, 1256, 1151, 1065, 1022, and 898 cm^{-1}),[41] and $[C_2mim][OAc]$ (1179 cm^{-1}) (see Figure S2a). The arrows indicate shifts in peak position.

GO. In this regard, rGO, being less hydrophilic than chitosan, may have interfered with chitosan chain interactions and recrystallization.

The B-series of materials also showed similar peaks to the A-series, but they were much less intense. The characteristic peak at 23.3° ascribed to the (110) lattice plane of the cellulose II crystalline structure for unprocessed CMC[26] was absent. This indicates that while processing had predominantly destroyed the original crystalline structures of both biopolymers, only the chitosan in the B-samples had undergone some degree of recrystallization. The recrystallized chitosan structure was formed with the assistance of $[C_2mim][OAc]$, as a predominantly amorphous material was obtained without plasticizer.[36] The effect of $[C_2mim][OAc]$ can also be confirmed by the slightly increased peak intensities (especially at 10, 13.6, and 21.8°) with increasing IL content from 20 to 40 wt %. Compared with BE2-F, BE2/GO-F displayed almost the same peak intensities while BE2/rGO-F showed more intense peaks at 10 and 13.6°. Compared with BE4-F, both BE4/GO-F and BE4/rGO-F exhibited greater peak intensities at 10 and 13.6°. This indicates that GO or rGO might have facilitated chitosan recrystallization.

Molecular Interactions. Figure 3a shows that the Fourier transform infrared (FTIR) spectra of the A-samples with 20 wt % $[C_2mim][OAc]$ were almost the same as that of A-F (processed chitosan film without plasticizer, reported previously).[26] The FTIR spectra of the A-samples with 20 and 40 wt % $[C_2mim][OAc]$ were very similar. The only difference was that the peak at 1179 cm^{-1}, derived from the imidazolium ring of the IL (see Figure S2a), was more pronounced (but with a red shift to 1169 cm^{-1}). The red shift of this peak reflects that a lower vibration energy is needed for the imidazolium ring when the IL interacted with the biopolymers.[37] Specifically, it is the acetate anion that interacts with biopolymer hydroxyl groups leading to dissolution or plasticization,[38−40] the interaction between the IL imidazolium cation and the acetate group was weakened because of the interactions between the acetate group and the biopolymer polar groups. No obvious shifts in the peaks for the biopolymers can be observed with addition of $[C_2mim][OAc]$. Moreover, the inclusion of GO or rGO did not cause any obvious changes to the FTIR bands, most likely due to the low GO or rGO content.

https://dx.doi.org/10.1021/acsomega.0c02418
ACS Omega XXXX, XXX, XXX−XXX

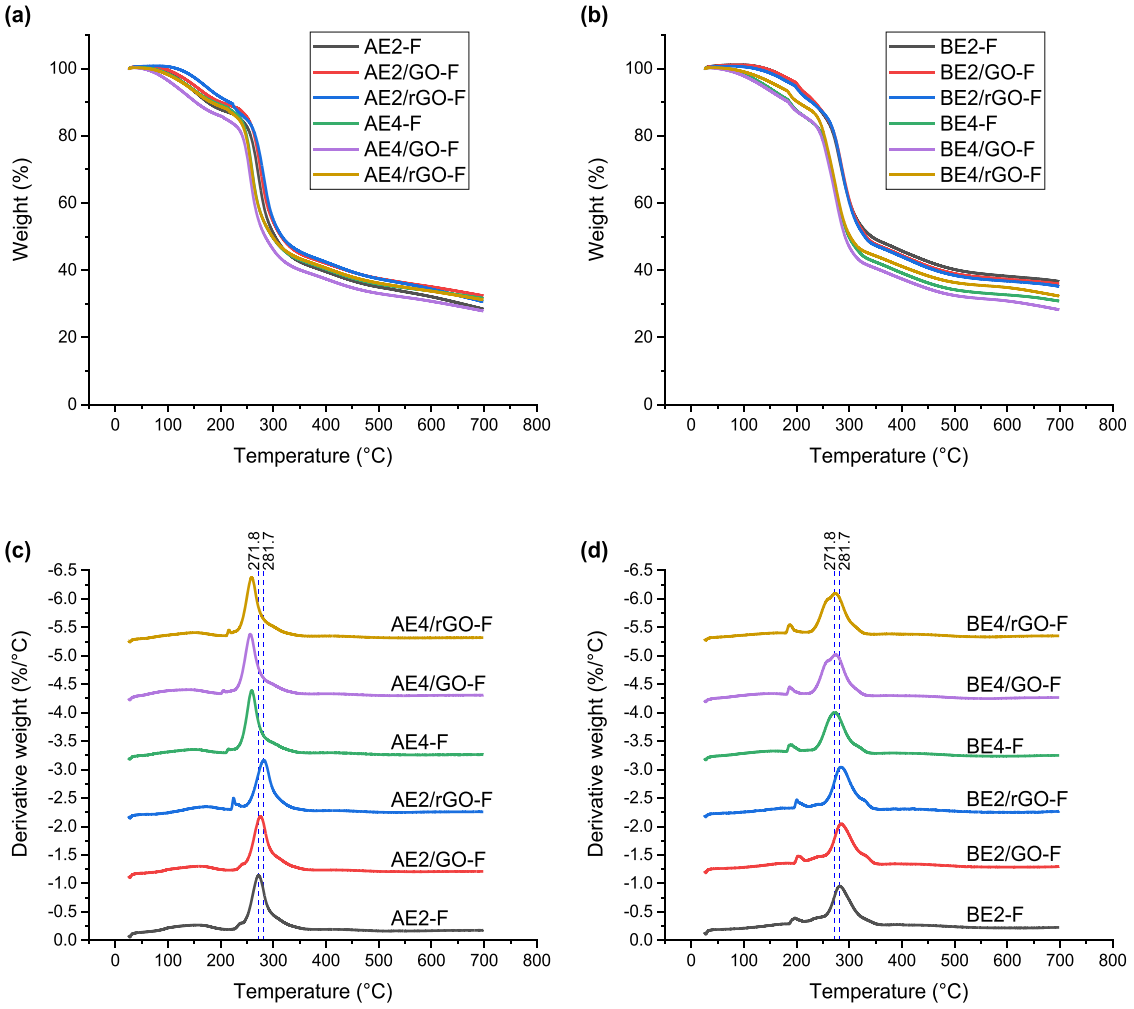

Figure 4. Weight percentage *vs* temperature curves ((a) chitosan matrix; (b) chitosan/CMC matrix) and derivative weight *vs* temperature curves ((c) chitosan matrix; (d) chitosan/CMC matrix) for the different biopolymer and bionanocomposite films. The reference lines indicate the major peak temperatures of BE2-F and AE2-F, respectively.

The B-series displayed FTIR spectra mostly similar to those for the A-series, although there were some changes in peak intensities. Derived from the CMC in the matrix, there was an additional reflection at 1414 cm^{-1} aligned to the asymmetric stretching vibration of carboxylate ions. The characteristic bands for CMC at 1055 cm^{-1} (C−O stretching vibration of ether groups) and 1589 cm^{-1} (symmetric stretching vibration of carboxylate ions)[42−45] may be overlapped by chitosan signals. Furthermore, there was a blue shift of the band originally at 1572 cm^{-1} (N−H bending from amine and amide II) and a red shift of the band originally at 1065 cm^{-1} (asymmetric C−O−C stretching in glycosidic linkage).[46−48] These shifts in band position confirm strong molecular interactions between the two complexed biopolymers. With a higher [C_2mim][OAc] content, the characteristic peak originally at 1179 cm^{-1} (shifted to 1169 cm^{-1}) became more intense, but no further band shifts for the biopolymers were observed. For the B-series, the addition of GO or rGO did not result in any discernible changes in the FTIR bands, perhaps not surprising given the GO/rGO loading was just 0.75 wt %.

Thermal Stability. Using thermogravimetric analysis (TGA), plots of weight percentage (Figure 4a,b) and derivative weight (Figure 4c,d) as a function of temperature for the different films were obtained. For all of the samples, there was a moderate weight loss before 200 °C, which could be mainly due to moisture loss. It can be seen from Figure 4a,b that among the A-series of samples, during this initial stage, AE2/rGO-F had the least weight loss, whereas AE4/GO-F had the most weight loss. Among the B-series of samples, those containing 40 wt % [C_2mim][OAc] experienced a greater weight loss than those containing 20 wt % [C_2mim][OAc] before 200 °C. These results indicate that a higher IL content led to a higher moisture content in the samples, which could be associated with the high hydrophobicity of the IL. GO and rGO, with different degrees of hydrophilicity/hydrophobicity, could also influence the moisture content in the samples.

Figure 4c,d shows that, for AE2-F, a shoulder process evolved at about 237 °C, due to the initial depolymerization of chitosan. This initial thermal decomposition event for thermomechanically processed chitosan has also been observed in previous studies.[26,36,49−51] The biggest transition occurred between 225 and 365 °C, undoubtedly attributed to the degradation of the biopolymer. The peak temperature (T_d, when the weight loss occurs at the maximum rate) of this major weight loss was 272 °C, much lower than that of A-F (297 °C), indicating that plasticization by [C_2mim][OAc] resulted in a decrease in the thermal stability of chitosan. Similarly, earlier studies[4,6] showed that [C_2mim][OAc] as a

https://dx.doi.org/10.1021/acsomega.0c02418
ACS Omega XXXX, XXX, XXX−XXX

plasticizer reduced the thermal stability of plasticized starch films. [C_2mim][OAc] had T_d = 252 °C (Figure S2b), which was much lower than that of unprocessed chitosan (296 °C).[41] The lower thermal stability of acetate ILs compared to ILs containing other anions like [Cl^-] has been well documented.[52] The radicals generated from the earlier thermal decomposition of the acetate anion (and the imidazolium cation) could possibly accelerate the chain scission of the biopolymer with increasing temperature. It is also possible that the IL promoted biopolymer chain degradation during thermomechanical processing.[8,9,11] The reduced thermal stability of biopolymers treated with ILs has been noted before.[4,53,54] With a higher [C_2mim][OAc] content, AE4-F displayed an even lower T_d value (259 °C), further testifying the effect the IL has in reducing the biopolymer thermal stability.

Compared to AE2-F, AE2/GO-F exhibited a slightly increased T_d value (276 °C) and AE2/rGO-F displayed an even higher T_d value (282 °C). In other words, both GO and rGO were effective at enhancing the thermal stability of chitosan. According to Stankovich et al.,[55] GO is relatively thermally unstable with the major mass loss occurring at about 200 °C presumably due to pyrolysis of the labile oxygen-containing functional groups, whereas rGO is more thermally stable. In line with this, our recent research[36] indicated that addition of GO decreased the T_d value of A-F (from 297 to 289 °C), whereas rGO addition resulted in increased T_d (to 307 °C). Here, the interaction between chitosan and GO possibly competed with that between chitosan and the acetate group of the IL, reducing the effect of [$OAc]^-$ and contributing to the decrease in the thermal stability of chitosan.

Compared to that of AE4-F (259 °C), the T_d value of AE4/rGO-F was unchanged, whereas the T_d value of AE4/GO-F was slightly reduced to 256 °C. It is possible that the plasticizer at higher content dominates the interaction with chitosan, while the interactions between chitosan and GO became insignificant. In this way, the low thermal stability of GO also led to reduced thermal stability of the whole composite matrix. Similarly, the positive effect of rGO at a higher [C_2mim][OAc] content became negligible.

BE2-F had T_d = 282 °C. Before the major peak, there was a small thermal decomposition event between 184 and 214 °C ascribed to the initial decomposition of the biopolymers. Overlapped with the main peak, there is another peak signifying an event at a higher temperature between 320 and 358 °C, associated with the polyelectrolyte complexed structure that was more resistant to thermal decomposition. Our previous work[26] showed that the major weight loss of thermomechanically processed chitosan/CMC without plasticizer (B-F) was composed of two pronounced overlapping peaks, the stronger one at 273 °C (T_d) and the weaker one at 304 °C. In comparison, BE2-F displayed a more-defined peak. The T_d value of BE2-F was also higher than that of AE2-F. Thus, the addition of [C_2mim][OAc] enhanced the thermal stability of the B-matrix possibly by assisting biopolymer chain mobility and then interactions between the two biopolymers.

Compared to BE2-F, BE2/GO-F and BE2/rGO-F had slightly higher T_d values (285 °C and 284 °C). The T_d value of BE4-F (272 °C) was less than that of BE2-F. Therefore, it is possible that PEC might become less effective with excess [C_2mim][OAc]. BE4/GO-F and BE4/rGO-F had T_d values similar to that of BE4-F. Nonetheless, for these two samples, there seemed to be an additional, overlapping peak at about 258−259 °C, which could be due to CMC. Likely, the combined effects of inclusion of GO or rGO and a high [C_2mim][OAc] content resulted in a lower degree of PEC and hydrogen bonding between chitosan and CMC so that the decomposition peak for CMC became more pronounced.

Molecular Relaxations. Figure 5 shows plots of loss tangent (tan δ) as a function of temperature for the films measured by dynamical mechanical thermal analysis (DMTA). All of the samples displayed two transitions, one at a lower temperature associated with a β-relaxation attributed to the motions of the side chains or lateral groups of chitosan and a much more prominent one at a higher temperature associated with the α-transition (glass transition) of chitosan.[56,57] For AE2-F, the peak temperatures of the β-transition (T_β) and α-transition (T_α) were about −28 and 73 °C, respectively. The T_β and T_α values of AE2-F were much lower than those of A-F (−47 and 119 °C, respectively),[26] suggesting that [C_2mim][OAc] readily plasticized the chitosan and increased chitosan chain mobility. AE2/GO-F and AE2/rGO-F displayed very similar tan δ profiles to that of AE2-F. In these samples, the chain mobility could be mainly determined by the IL, whereas the effect of GO or rGO was minor.

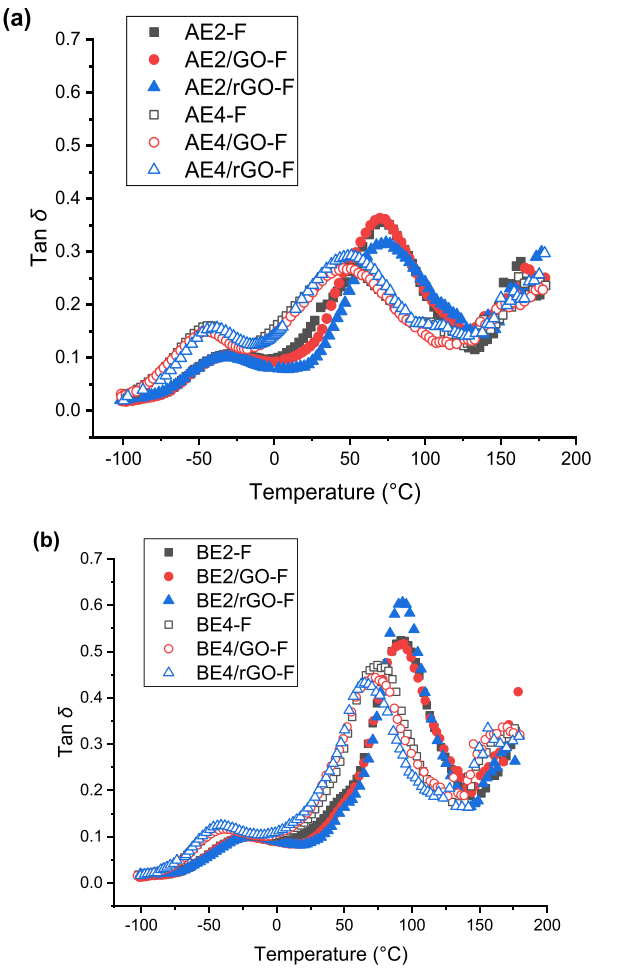

Figure 5. Damping (tan δ) as a function of temperature for the different biopolymer and bionanocomposite films: (a) chitosan matrix; (b) chitosan/CMC matrix.

https://dx.doi.org/10.1021/acsomega.0c02418
ACS Omega XXXX, XXX, XXX−XXX

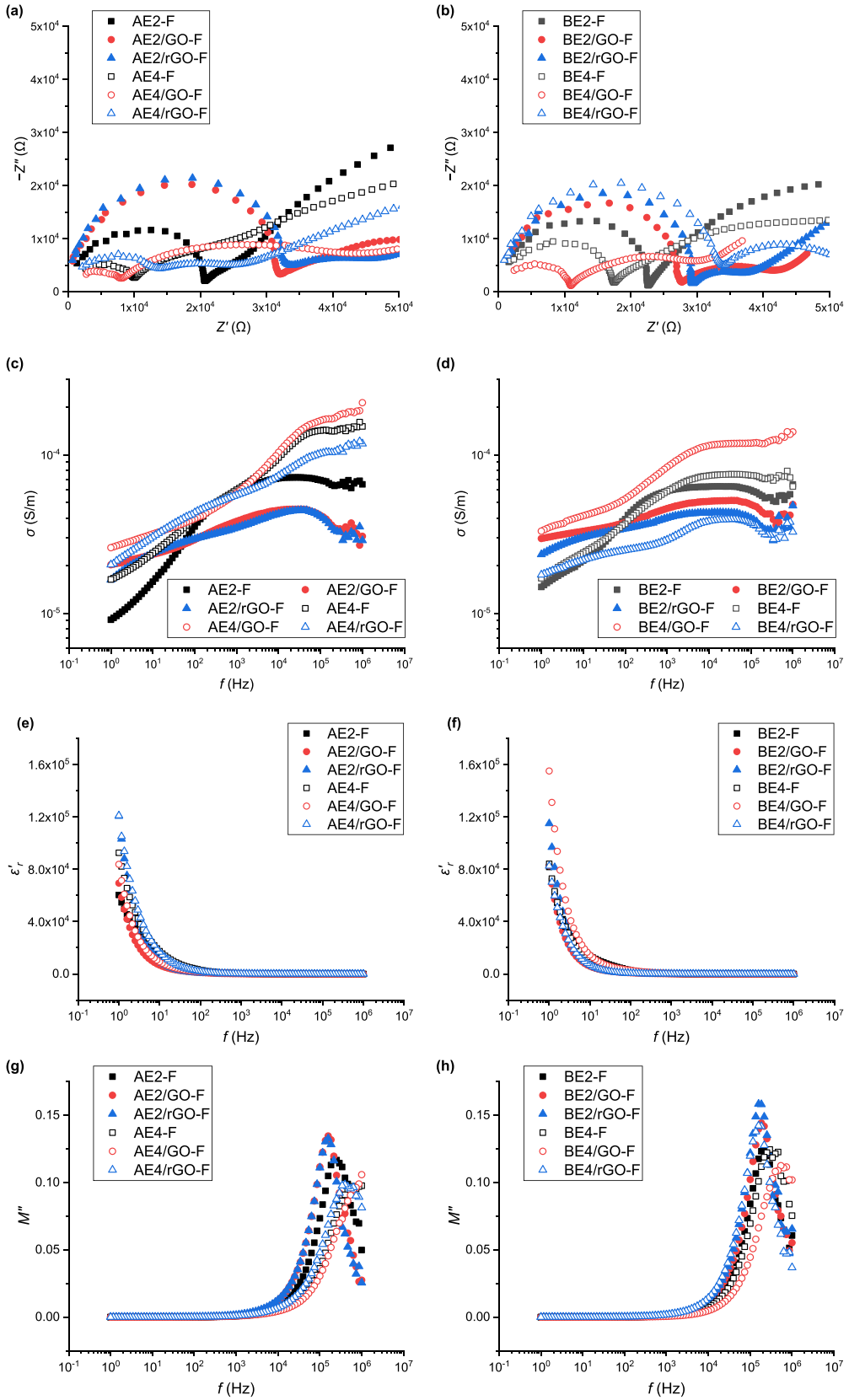

Figure 6. EIS results of the different biopolymer and bionanocomposite films: (a, b) Nyquist plot of impedance; (c, d) alternating current (AC) conductivity (σ); (e, f) real relative permittivity (ε'_r); and (g, h) imaginary electric modulus (M'').

With a higher (40 wt %) [C_2mim][OAc] content, both T_β and T_α were significantly reduced. AE4-F had $T_\beta = -42$ °C and $T_\alpha = 46$ °C. AE4/GO-F had similar T_β and T_α values to those of AE4-F while the T_α value of AE4/rGO-F was slightly higher (51 °C), possibly due to the confinement effect of rGO on chitosan chain mobility.

https://dx.doi.org/10.1021/acsomega.0c02418
ACS Omega XXXX, XXX, XXX−XXX

BE2-F had T_β = −23 °C and T_α = 91 °C, which appeared not to be changed by addition of GO or rGO. These values were higher than those for the A-samples with 20% [C_2mim][OAc], suggesting that PEC restricted the biopolymer chain mobility. BE4-F had T_β = −38 °C and T_α = 74 °C, with the greater [C_2mim][OAc] content resulting in a higher chain mobility. Interestingly, inclusion of GO or rGO to the plasticized B-series materials further reduced the relaxation temperatures. BE2/GO-F had T_β = −38 °C and T_α = 72 °C, and BE2/rGO-F had T_β = −41 °C and T_α = 66 °C. It may be that rGO interfered with PEC between the two biopolymers, leading to increased chain mobility.

Electrochemical Impedance Spectroscopy (EIS). Figure 6a,b shows the Nyquist plots of Z'' *vs* Z', consisting of a half semicircle at high frequencies (f) characteristic of a combination of bulk resistance and bulk capacitance in parallel.[58] A larger semicircular is indicative of greater bulk resistance. Based on these plots, the values of bulk resistance (R_b) and ionic conductivity (σ_{dc})[58] calculated are listed in Table S1. Overall, σ_{dc} was strongly affected by the [C_2mim][OAc] content and GO or rGO addition. The highest σ_{dc} value was displayed by the samples with 40 wt % [C_2mim][OAc]. While electrical conductivity in polymer systems is determined by electrical charges (ions and dipoles), [C_2mim][OAc] as a salt can also play an important role here.[59] The σ_{dc} value of AE4-F ((13.33 ± 4.26) × 10^5 S·m^{-1}) was higher than that of BE4-F ((7.30 ± 2.91) × 10^5 S·m^{-1}), as expected, as PEC could negatively influence ionic conductivity. Addition of GO to AE4-F or BE4-F resulted in an even higher σ_{dc} (*e.g.*, (17.77 ± 0.72) × 10^5 S·m^{-1} for AE4/GO-F), while rGO led to a reduced σ_{dc} (*e.g.*, (3.70 ± 0.69) × 10^5 S·m^{-1} for BE4/rGO-F). Given this, it is possible that GO, by interaction with the biopolymer, reduced the interactions between [C_2mim][OAc] and the biopolymer, leading to more free IL ions available for conduction. In contrast, rGO disrupts PEC and/or hydrogen bonding between biopolymer chains, increasing the chances the IL interacts with the biopolymer, reducing the concentration of free IL ions. When the IL content is low (20 wt %), the interaction between the IL and GO predominates, which could alter the conductivity.

Figure 6c,d shows that for all of the samples, AC conductivity (σ) increased with f, typical behavior of an insulating material (*i.e.*, a dielectric). Low σ at low f results from the accumulation of charged species at the electrode−electrolyte interface and, thus, less mobile ions in the bulk material.[60] AE2-F had particularly low σ values at low f, but σ increased sharply at higher f. In contrast, for AE2/GO-F and AE2/rGO-F, the σ values at low f were higher and σ was less dependent on f. All of the A-samples with 40% [C_2mim][OAc] had high σ values across the whole f range, due to more mobile ions in the systems. While the B-samples with 20% [C_2mim][OAc] displayed similar behavior, a higher IL content (40%) did not significantly increase σ. Also, the height of the σ curve was largely influenced by GO or rGO, in agreement with the discussion on σ_{dc} above.

Figure 6e,f shows that for all samples, the real relative permittivity (ε'_r) abruptly increased with decreasing f, attributable to electrode polarization and space charge effects (dipole moment).[61,62] Among the different samples, those containing rGO exhibited the highest ε'_r at low f. In this regard, the relatively more electrically conducting rGO might assist in the accumulation of mobile ions. Moreover, all of the samples had impressively high ε'_r, as listed in Table S1. The highest ε'_r values at 1 kHz were for AE4/GO-F (432 ± 49) and BE4/GO-F (380 ± 130), much higher than those for most polymer nanocomposites (normally below 50 at 1 kHz) for energy applications.[63−65]

Figure 6g,h shows that imaginary electric modulus (M'') abruptly increased with f higher than 10^3 Hz. For the A-samples with 20% [C_2mim][OAc], a well-defined peak evolved, indicating relaxation processes with a distribution of relaxation times (*i.e.*, viscoelastic relaxation or dipolar relaxation).[66] Compared with AE2-F, AE2/GO-F and AE2/rGO-F displayed a more intensive peak at lower f. In this regard, inclusion of GO or rGO decreased biopolymer chain mobility, making ions and associated dipoles less mobile. In contrast, for a higher [C_2mim][OAc] content, the peak shifts to a higher f as the IL facilitates biopolymer chain movement and increased mobility of ions and associated dipoles. Compared with AE4-F, AE4/rGO showed the M'' peak at a slightly lower f, whereas for AE4/GO-F, M'' kept increasing up to the highest f tested. This could be linked to the effect of the nanofiller on the availability of free, mobile ions, and dipoles in the samples, as already proved in the discussion on σ_{dc}.

All of the B-samples with 20% [C_2mim][OAc] displayed a relaxation peak in M'' at similar f. In comparison, for BE4-F, the peak moved to higher f. Excess [C_2mim][OAc] disturbs PEC, resulting in increased chain, ionic, and dipole mobilities. BE4/rGO-F displayed the M'' peak at a lower f, whereas, for BE4/GO-F, the peak further moved to higher f, as the case for AE4/GO-F.

Mechanical Properties. The Young's modulus (E), tensile strength (σ_t), and elongation at break (ε_b) of the different samples were calculated; see Figure 7. Overall, the [C_2mim][OAc] content influenced the tensile properties more than GO or rGO addition, perhaps unsurprising given the relatively low loading at 0.75 wt %. The samples with 20 wt % [C_2mim][OAc] had notably higher E and σ_t but lower ε_b than those with 40 wt % [C_2mim][OAc] content. The highest σ_t was displayed by the B-matrix with 20 wt % [C_2mim][OAc] (*e.g.*, for BE2-F, 39.1 ± 2.6 MPa), which could be ascribed to PEC between the two biopolymers. At a higher IL content, biopolymer chain interactions and entanglements are reduced, resulting in diminished mechanical properties. For the B-matrix with 40 wt % [C_2mim][OAc], addition of GO or rGO further decreased E and σ_t, suggesting possibly weakened PEC. For either A- or B-matrix with 20 wt % [C_2mim][OAc], addition of rGO only led to an increase in E (for AE2/rGO, 1011 ± 68 MPa; and for BE2/rGO, 1018 ± 100 MPa), while addition of GO resulted in decreases in σ_t and ε_b for AE2/GO-F. Previously, we reported that addition of GO or rGO to both A-F and B-F yielded increased mechanical properties.[36] In this instance, the presence of the IL significantly reduces the interactions between GO or rGO and the biopolymer matrix. The greatest effect was observed for the A-samples with 40 wt % [C_2mim][OAc] content, which showed the lowest E and σ_t (*e.g.*, for AE4-F, E = 101 ± 15 MPa, σ_t = 11.6 ± 1.3 MPa)

Contact Angle. The surface hydrophilicity of films is represented by contact angle values at 0 s and 60 s (θ_{c0s} and θ_{c60s}), as shown in Figure 8. Compared with A-F (θ_{c0s} = 90 ± 5° and θ_{c60s} = 68 ± 5°),[26] AE2-F had decreased surface hydrophilicity with θ_{c0s} = 100 ± 7° and θ_{c60s} = 71 ± 10°, *i.e.*, the surface of this sample became more hydrophobic and not expected given the high hydrophilicity of ILs. A previous study[8] reported the significantly lower hydrophilicity of thermoplastic starch plasticized by 1-butyl-3-methylimidazo-

https://dx.doi.org/10.1021/acsomega.0c02418
ACS Omega XXXX, XXX, XXX−XXX

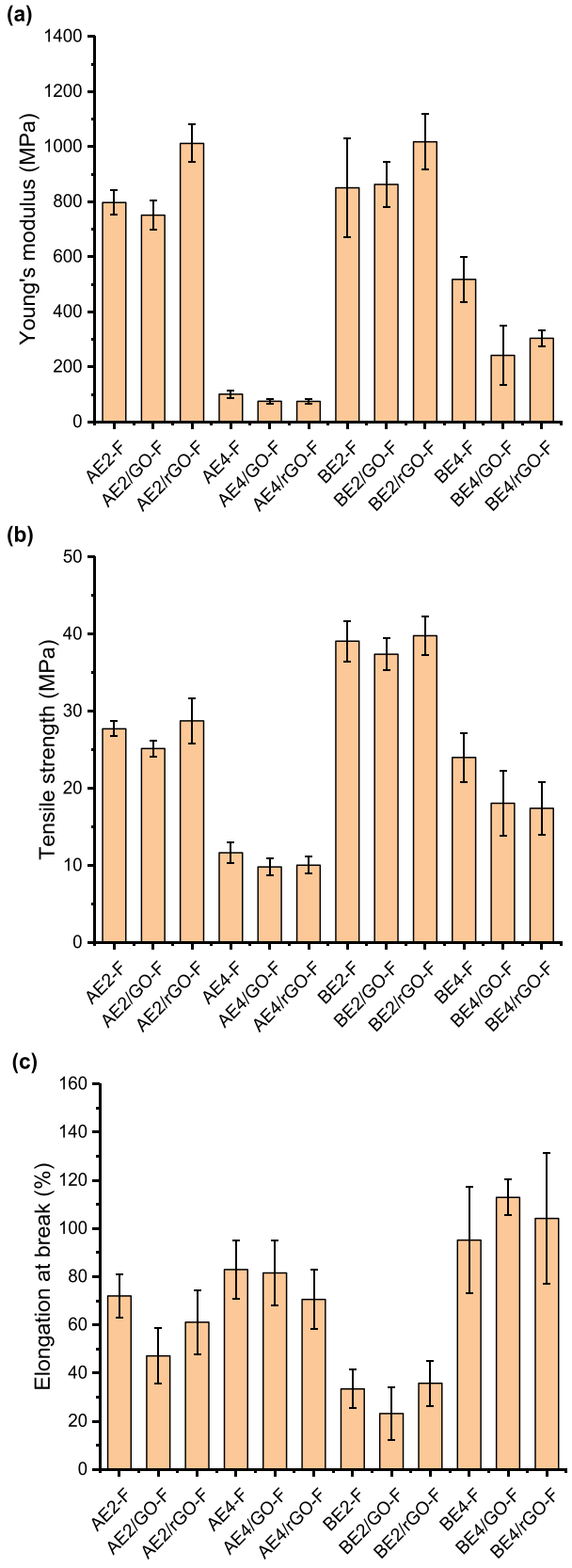

Figure 7. (a) Young's modulus, (b) tensile strength, and (c) elongation at break of the different biopolymer and composite films. The error bars represent standard deviations.

lium chloride ([C_4mim]Cl) compared to glycerol. In this work, we speculate that the strong hydrogen-bonding interaction between chitosan and [C_2mim][OAc] reduces the availability of the hydroxyl groups from chitosan or the IL ions to bind with water molecules, especially at the immediate start of the sessile measurement. The inclusion of GO or rGO increased the surface hydrophilicity, with the effect being greater with rGO. The values of θ_{c0s} and θ_{c60s} for AE2/rGO-F were similar to those reported previously for A-F.[26] Therefore, GO or rGO may disrupt the hydrogen bonding between chitosan chains, making more hydroxyl groups available to interact with water.

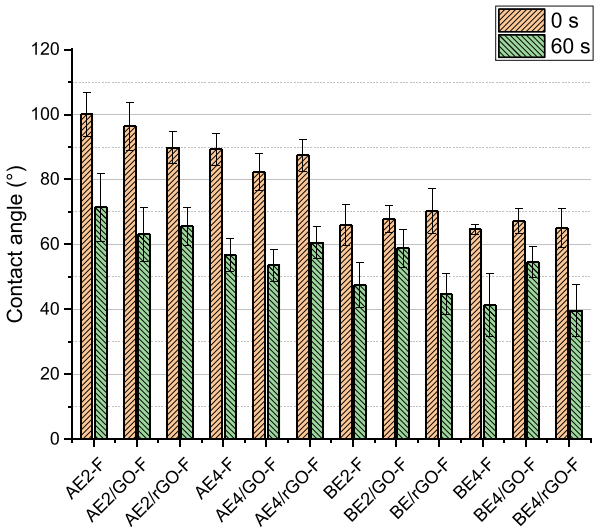

Figure 8. Contact angle values for the different biopolymer and bionanocomposite films at 0 and 60 s. The error bars represent standard deviations.

Compared to those for AE2-F, the θ_{c0s} and θ_{c60s} values for AE4-F were reduced. The increased surface hydrophilicity could be due to excess [C_2mim][OAc] in the composite system, which is free to bind with water molecules. The addition of GO slightly reduced θ_{c0s} and θ_{c60s}, while rGO led to slightly increased θ_{c60s}, a behavior related to the difference in hydrophilicity/hydrophobicity of the surfaces of GO and rGO, the latter more hydrophobic.

For B-F, $\theta_{c0s} = 71 \pm 6°$ and $\theta_{c60s} = 60 \pm 5°$.[26] The presence of the CMC sodium salt obviously contributed to increased surface hydrophilicity of the matrix, most likely due to the carboxyl groups and Na^+ ions. When plasticized by [C_2mim][OAc], BE-F exhibited lower θ_{c0s} and θ_{c60s} values (66 ± 6 and 47 ± 7) than those of B-F. Further addition of GO led to increased θ_{c60s}, while the effect of rGO was insignificant. In this regard, the interaction between GO and the IL may reduce the interaction of IL ions with water. Compared with AE2-F, AE4-F exhibited further reduced θ_{c60s}. To this matrix, the addition of rGO was not effective, whereas GO notably increased θ_{c60s}, which, again, can be ascribed to the interaction between GO and the IL.

CONCLUSIONS

There are several interactions among different components in chitosan and chitosan/CMC polyelectrolyte complexed bionanocomposites, as summarized below:

(1) GO and rGO were effectively dispersed in both matrices by thermomechanical mixing. However, the influence of GO/rGO on the structure and properties of the bionanocomposites is largely dependent on the [C_2mim][OAc] content.

https://dx.doi.org/10.1021/acsomega.0c02418
ACS Omega XXXX, XXX, XXX−XXX

(2) [C_2mim][OAc] acts as a plasticizer and had the dominant effect on the structure and properties of the bionanocomposites. The presence of the IL increased the mobility of the biopolymer chains as well as IL ions and associated dipoles, reducing chain interactions and entanglements, biopolymer crystallinity, and thermal stability. This resulted in the bionanocomposites having higher ionic conductivity, shorter electrical relaxation times, and reduced stiffness and strength, but greater ductility.

(3) PEC between the biopolymers resulted in reduced biopolymer chain mobility, higher mechanical strength, rigidity, and thermal stability but lower ion conductivity. However, PEC was strongly affected by the efficacy of IL plasticization and inclusion of GO/rGO.

Thus, this study shows that the structure and properties of bionanocomposites are not just determined by the surface chemistry of GO/rGO but can also be influenced by multiple interactions involving plasticizers such as ILs and additional biopolymers. The new information obtained here could guide the rational design of such materials with competitive properties.

EXPERIMENTAL SECTION

Materials. Chitosan (poly(β-(1,4)-D-glucosamine)), derived from crab shells, with a weight-average molecular mass (M_w) of about 150 000 g·mol^{-1}, a degree of deacetylation (DD) of >90%, and a viscosity of about 100 mPa·s (*i.e.*, 1% solution in 1% acetic acid at 25 °C), was purchased from Shanghai Ryon Biological Technology Co., Ltd. (China). The characteristics of this chitosan are shown in our previous study.[41] CMC sodium, with an M_w value of 90 000 g·mol^{-1}, a degree of substitution (DS) of 0.7, and a viscosity of 50−100 mPa·s (Brookfield, 2% solution, at 25 °C), was purchased from Shanghai Macklin Biochemical Co., Ltd. (China). This CMC was characterized previously.[26] GO (aqueous acid paste with 25% GO, 74% water, and 1−1.5% HCl) was purchased from Abalonyx AS (Norway). Hydrazine hydrate solution (78−82% iodometric, Honeywell Fluka) and ammonia solution (35%, AR, d = 0.88) were supplied by Fisher Scientific U.K. Ltd.; [C_2mim][OAc] (≥95.0%) by Sigma-Aldrich Company Ltd. (U.K.); and formic acid (98% w/w AR) and NaBr (pure) were supplied by Scientific Laboratory Supplies Ltd. (U.K.). Deionized water was used for all experiments.

Synthesis of Reduced Graphene Oxide (rGO). rGO was synthesized from GO as described previously.[36] Briefly, a mixture of 40 g of the GO paste (25 wt % concentration, used as received), 150 mL of distilled water, 25 mL of the hydrazine hydrate solution, and 25 mL of the ammonia solution (both used as received) in a round-bottom flask was heated at 90 °C for 4 h with magnetic stirring under reflux. After this reaction, this mixture was filtered and washed with water to reach neutral pH, followed by drying in a vacuum oven. For the powder product obtained, the same procedure was performed once again to ensure adequate reaction.

Sample Preparation. Table 1 shows the formulations and codes of the different samples prepared in this work. In these codes, the prefix "A" represents chitosan alone as the matrix while "B" indicates chitosan/CMC as the matrix. The suffix "F" indicates the processed samples as films. The [C_2mim][OAc] content is represented by the letter "E" followed by a number, for example, "E2" for 20 wt % [C_2mim][OAc]. The samples were prepared by preblending, thermomechanical kneading, hot-pressing, and then conditioning, as described previously,[26] except that the GO or rGO and [C_2mim][OAc] were added during the preblending stage.

Table 1. Sample Codes and Compositions Used in This Study (Represented as Portions by Weight)

sample	chitosan	CMC	[C_2mim][OAc]	GO	rGO	2 M formic acid solution
AE2-F	100		20			261
AE2/GO-F	100		20	0.75		261
AE2/rGO-F	100		20		0.75	261
AE4-F	100		40			261
AE4/GO-F	100		40	0.75		261
AE4/rGO-F	100		40		0.75	261
BE2-F	50	50	20			261
BE2/GO-F	50	50	20	0.75		261
BE2/rGO-F	50	50	20		0.75	261
BE4-F	50	50	40			261
BE4/GO-F	50	50	40	0.75		261
BE4/rGO-F	50	50	40		0.75	261

Characterization. Scanning electron microscopy (SEM) was performed using a ZEISS SIGMA field emission scanning electron microscope at 6 kV. The samples were prepared by cryo-fracturing films under liquid nitrogen cooling and sputter-coated with gold/palladium.

Scanning transmission electron microscopy (STEM) was conducted using a field emission gun Talos F200X transmission electron microscope operating at 200 kV, in which both STEM bright-field (BF) and high-angle annular dark-field (HAADF) images were acquired simultaneously. Sample ribbons, about 60 nm thick, were sectioned from epoxy-embedded sample blocks and subsequently transferred on to 200-mesh copper grids coated with holey carbon films. No liquid solution was involved, to avoid potential damage to the samples.

X-ray diffractograms were acquired using a PANalytical Empyrean X-ray diffractometer with a Co target (Kα = 1.790307 Å) and a beam slit of 10 mm at 40 kV and 40 mA. The samples were scanned over an angular range (2θ) of 6−40° with a step size of 0.0263° and a scan rate of 2.16 s·step^{-1}.

Fourier transform infrared (FTIR) spectra were collected using a Bruker TENSOR 27 FTIR spectrometer with an attenuated total reflection (ATR) accessory with 32 scans for each sample over a range of 4000−500 cm^{-1} at room temperature (RT).

Thermogravimetric analysis (TGA) was undertaken using a Mettler Toledo TGA apparatus over a temperature range of 30−700 °C at 10 K·min^{-1} under nitrogen.

Dynamic mechanical thermal analysis (DMTA) was performed using a Tritec 2000 DMA (Triton Technology Ltd., U.K.) in the dual cantilever mode with a sample length of 5 mm at a displacement of 0.01 mm. Temperature scans were performed from −100 °C to 180 °C at 2 K·min^{-1} and 1 Hz. Frequency scans were conducted from 0.01 to 20 Hz at RT.

Electrical impedance spectroscopy (EIS) was performed using a Princeton Applied Research PARSTAT MC (PMC) multichannel potentiostat (Ametek Scientific Instrument) with a PMC-2000 card and a two-point probe. The two surfaces of samples were painted with carbon conductive grease (No. 8481, MG Chemicals, Canada) in designated areas (24 × 24 mm^2). All tests were performed in triplicate. The real (Z') and

https://dx.doi.org/10.1021/acsomega.0c02418
ACS Omega XXXX, XXX, XXX−XXX

imaginary (Z'') parts of impedance were acquired with a frequency (f) range of $1-10^6$ Hz. The AC conductivity (admittance) (σ), the real part of relative permittivity (ε'_r), and the imaginary part of electric modulus (M'') were calculated using the following equations[60,67,68]

$$\sigma = \frac{Z'}{Z'^2 + Z''^2} \times \frac{t}{A} \quad (1)$$

$$\varepsilon'_r = \frac{-Z''}{Z'^2 + Z''^2} \times \frac{t}{\omega A \varepsilon_0} \quad (2)$$

$$M'' = \frac{\varepsilon''}{\varepsilon'^2 + \varepsilon''^2} \quad (3)$$

where ω is the angular frequency ($=2\pi f$), ε_0 is the permittivity of free space ($\approx 8.854 \times 10^{-12}$ F·m^{-1}), A is the tested area of the sample (m^2), and t is the sample thickness (m).

The bulk resistance (R_b) was determined from the Nyquist plots of impedance (Z'' *vs* Z') from the points where the semicircle and the straight line meet. Then, the conductivity (σ_{dc}) can be calculated using eq 4[60,66]

$$\sigma_{dc} = \frac{t}{R_b \times A} \quad (4)$$

Tensile testing (at least seven replicates) was performed using an Instron 3367 universal testing machine with a 1 kN load cell and a crosshead speed of 3 mm/min. As the specimens were in the form of thin sheets, specimen extension was measured by grip separation, as suggested by ASTM Standard D882.

Contact angle (θ_c) data were obtained from sessile tests at RT based on the Young–Laplace equation using an Attension Theta Lite instrument (Biolin Scientific, U.K.).

■ ASSOCIATED CONTENT

Supporting Information

The Supporting Information is available free of charge at https://pubs.acs.org/doi/10.1021/acsomega.0c02418.

FTIR spectrum and TGA result of [C_2mim][OAc] (Figure S2); SEM images (Figure S1), representative stress–strain curves (Figure S3), Shore D hardness (Figure S4), and electrochemical results (Table S1) of the different biopolymer films; and notes to figures (PDF)

■ AUTHOR INFORMATION

Corresponding Authors

Fengwei Xie – *International Institute for Nanocomposites Manufacturing (IINM), WMG, University of Warwick, Coventry CV4 7AL, United Kingdom; School of Chemical Engineering, The University of Queensland, Brisbane, Qld 4072, Australia;* orcid.org/0000-0002-2033-082X; Email: d.xie.2@warwick.ac.uk, fwhsieh@gmail.com

Tony McNally – *International Institute for Nanocomposites Manufacturing (IINM), WMG, University of Warwick, Coventry CV4 7AL, United Kingdom;* orcid.org/0000-0001-5436-4211; Email: t.mcnally@warwick.ac.uk

Authors

Pei Chen – *College of Food Science, South China Agricultural University, Guangzhou, Guangdong 510642, China; International Institute for Nanocomposites Manufacturing (IINM), WMG, University of Warwick, Coventry CV4 7AL, United Kingdom*

Fengzai Tang – *WMG, University of Warwick, Coventry CV4 7AL, United Kingdom*

Complete contact information is available at: https://pubs.acs.org/10.1021/acsomega.0c02418

Author Contributions

All authors have given approval to the final version of the manuscript. F.X. led the research.

Notes

The authors declare no competing financial interest.

■ ACKNOWLEDGMENTS

The authors acknowledge funding from the European Union's Horizon 2020 research and innovation program under the Marie Skłodowska-Curie grant agreement no. 798225. P.C. acknowledges the financial support from the China Scholarship Council (CSC) for her visiting position and thanks IINM, WMG, University of Warwick, U.K., for hosting her research visit. F.X. also acknowledges support from the Guangxi Key Laboratory for Polysaccharide Materials and Modification, Guangxi University for Nationalities, China (grant no. GXPSMM18ZD-02).

■ ABBREVIATIONS USED

CMC, carboxymethyl cellulose; GO, graphene oxide; rGO, reduced graphene oxide; PEC, polyelectrolyte complexation; IL, ionic liquid; [C_2mim][OAc], 1-ethyl-3-methylimidazolium acetate; T_d, thermal decomposition temperature at maximum weight loss rate; tan δ, loss tangent; T_β, peak temperature of β-transition; T_α, peak temperature of α-transition; θ_{c0s}, contact angle at 0 s; θ_{c60s}, contact angle at 60 s

■ REFERENCES

(1) Song, J.; Chen, C.; Zhu, S.; Zhu, M.; Dai, J.; Ray, U.; Li, Y.; Kuang, Y.; Li, Y.; Quispe, N.; Yao, Y.; Gong, A.; Leiste, U. H.; Bruck, H. A.; Zhu, J. Y.; Vellore, A.; Li, H.; Minus, M. L.; Jia, Z.; Martini, A.; Li, T.; Hu, L. Processing bulk natural wood into a high-performance structural material. *Nature* **2018**, *554*, 224.

(2) Frey, M.; Widner, D.; Segmehl, J. S.; Casdorff, K.; Keplinger, T.; Burgert, I. Delignified and Densified Cellulose Bulk Materials with Excellent Tensile Properties for Sustainable Engineering. *ACS Appl. Mater. Interfaces* **2018**, *10*, 5030–5037.

(3) Fang, Z.; Li, B.; Liu, Y.; Zhu, J.; Li, G.; Hou, G.; Zhou, J.; Qiu, X. Critical Role of Degree of Polymerization of Cellulose in Super-Strong Nanocellulose Films. *Matter* **2020**, *2*, 1000–1014.

(4) Xie, F.; Flanagan, B. M.; Li, M.; Sangwan, P.; Truss, R. W.; Halley, P. J.; Strounina, E. V.; Whittaker, A. K.; Gidley, M. J.; Dean, K. M.; Shamshina, J. L.; Rogers, R. D.; McNally, T. Characteristics of starch-based films plasticised by glycerol and by the ionic liquid 1-ethyl-3-methylimidazolium acetate: a comparative study. *Carbohydr. Polym.* **2014**, *111*, 841–848.

(5) Xie, F.; Flanagan, B. M.; Li, M.; Truss, R. W.; Halley, P. J.; Gidley, M. J.; McNally, T.; Shamshina, J. L.; Rogers, R. D. Characteristics of starch-based films with different amylose contents plasticised by 1-ethyl-3-methylimidazolium acetate. *Carbohydr. Polym.* **2015**, *122*, 160–168.

(6) Zhang, B.; Xie, F.; Zhang, T.; Chen, L.; Li, X.; Truss, R. W.; Halley, P. J.; Shamshina, J. L.; McNally, T.; Rogers, R. D. Different characteristic effects of ageing on starch-based films plasticised by 1-ethyl-3-methylimidazolium acetate and by glycerol. *Carbohydr. Polym.* **2016**, *146*, 67–79.

(7) Zhang, B.; Xie, F.; Shamshina, J. L.; Rogers, R. D.; McNally, T.; Wang, D. K.; Halley, P. J.; Truss, R. W.; Zhao, S.; Chen, L. Facile

Preparation of Starch-Based Electroconductive Films with Ionic Liquid. *ACS Sustainable Chem. Eng.* **2017**, *5*, 5457−5467.
(8) Sankri, A.; Arhaliass, A.; Dez, I.; Gaumont, A. C.; Grohens, Y.; Lourdin, D.; Pillin, I.; Rolland-Sabaté, A.; Leroy, E. Thermoplastic starch plasticized by an ionic liquid. *Carbohydr. Polym.* **2010**, *82*, 256−263.
(9) Leroy, E.; Jacquet, P.; Coativy, G.; Reguerre, Al.; Lourdin, D. Compatibilization of starch−zein melt processed blends by an ionic liquid used as plasticizer. *Carbohydr. Polym.* **2012**, *89*, 955−963.
(10) Colomines, G.; Decaen, P.; Lourdin, D.; Leroy, E. Biofriendly ionic liquids for starch plasticization: a screening approach. *RSC Adv.* **2016**, *6*, 90331−90337.
(11) Decaen, P.; Rolland-Sabaté, A.; Guilois, S.; Jury, V.; Allanic, N.; Colomines, G.; Lourdin, D.; Leroy, E. Choline chloride vs choline ionic liquids for starch thermoplasticization. *Carbohydr. Polym.* **2017**, *177*, 424−432.
(12) Ren, F.; Wang, J.; Xie, F.; Zan, K.; Wang, S.; Wang, S. Applications of ionic liquids in starch chemistry: a review. *Green Chem.* **2020**, *22*, 2162−2183.
(13) Ning, W.; Zhang, X.; Wang, X.; Liu, H. Ionic liquids modified montmorillonite/thermoplastic starch nanocomposites as ionic conducting biopolymer. *Macromol. Res.* **2009**, *17*, 285−288.
(14) Ning, W.; Zhang, X.; Liu, H.; He, B. 1-Allyl-3-methylimidazolium chloride plasticized-corn starch as solid biopolymer electrolytes. *Carbohydr. Polym.* **2009**, *76*, 482−484.
(15) Ning, W.; Zhang, X.; Liu, H.; Han, N. Ionically conducting polymers based on ionic liquid-plasticized starch containing lithium chloride. *Polym. Polym. Compos.* **2010**, *18*, 53−58.
(16) Ramesh, S.; Liew, C.-W.; Arof, A. K. Ion conducting corn starch biopolymer electrolytes doped with ionic liquid 1-butyl-3-methylimidazolium hexafluorophosphate. *J. Non-Cryst. Solids* **2011**, *357*, 3654−3660.
(17) Ramesh, S.; Shanti, R.; Morris, E.; Durairaj, R. Utilisation of Corn Starch in Production of 'green' Polymer Electrolytes. *Mater. Res. Innovations* **2011**, *15*, s13−s8.
(18) Ramesh, S.; Shanti, R.; Morris, E. Studies on the thermal behavior of CS:LiTFSI:[Amim] Cl polymer electrolytes exerted by different [Amim] Cl content. *Solid State Sci.* **2012**, *14*, 182−186.
(19) Liew, C.-W.; Ramesh, S. Electrical, structural, thermal and electrochemical properties of corn starch-based biopolymer electrolytes. *Carbohydr. Polym.* **2015**, *124*, 222−228.
(20) Liew, C.-W.; Ramesh, S.; Ramesh, K.; Arof, A. Preparation and characterization of lithium ion conducting ionic liquid-based biodegradable corn starch polymer electrolytes. *J. Solid State Electrochem.* **2012**, *16*, 1869−1875.
(21) Wang, H.; Gurau, G.; Rogers, R. D. Ionic liquid processing of cellulose. *Chem. Soc. Rev.* **2012**, *41*, 1519−1537.
(22) Li, Z.; Ramay, H. R.; Hauch, K. D.; Xiao, D.; Zhang, M. Chitosan−alginate hybrid scaffolds for bone tissue engineering. *Biomaterials* **2005**, *26*, 3919−3928.
(23) Wei, C.; Zhu, X.; Peng, H.; Chen, J.; Zhang, F.; Zhao, Q. Facile Preparation of Lignin-Based Underwater Adhesives with Improved Performances. *ACS Sustainable Chem. Eng.* **2019**, *7*, 4508−4514.
(24) Meng, L.; Xie, F.; Zhang, B.; Wang, D. K.; Yu, L. Natural Biopolymer Alloys with Superior Mechanical Properties. *ACS Sustainable Chem. Eng.* **2019**, *7*, 2792−2802.
(25) Basu, S.; Plucinski, A.; Catchmark, J. M. Sustainable barrier materials based on polysaccharide polyelectrolyte complexes. *Green Chem.* **2017**, *19*, 4080−4092.
(26) Chen, P.; Xie, F.; Tang, F.; McNally, T. Thermomechanical-induced polyelectrolyte complexation between chitosan and carboxymethyl cellulose enabling unexpected hydrolytic stability. *Compos. Sci. Technol.* **2020**, *189*, No. 108031.
(27) Iwasaki, N.; Yamane, S.-T.; Majima, T.; Kasahara, Y.; Minami, A.; Harada, K.; Nonaka, S.; Maekawa, N.; Tamura, H.; Tokura, S.; Shiono, M.; Monde, K.; Nishimura, S.-I. Feasibility of Polysaccharide Hybrid Materials for Scaffolds in Cartilage Tissue Engineering: Evaluation of Chondrocyte Adhesion to Polyion Complex Fibers Prepared from Alginate and Chitosan. *Biomacromolecules* **2004**, *5*, 828−833.
(28) Yang, X.; Tu, Y.; Li, L.; Shang, S.; Tao, X.-m. Well-Dispersed Chitosan/Graphene Oxide Nanocomposites. *ACS Appl. Mater. Interfaces* **2010**, *2*, 1707−1713.
(29) Kuilla, T.; Bhadra, S.; Yao, D.; Kim, N. H.; Bose, S.; Lee, J. H. Recent advances in graphene based polymer composites. *Prog. Polym. Sci.* **2010**, *35*, 1350−1375.
(30) Chen, J.; Peng, H.; Wang, X.; Shao, F.; Yuan, Z.; Han, H. Graphene oxide exhibits broad-spectrum antimicrobial activity against bacterial phytopathogens and fungal conidia by intertwining and membrane perturbation. *Nanoscale* **2014**, *6*, 1879−1889.
(31) Perreault, F.; de Faria, A. F.; Nejati, S.; Elimelech, M. Antimicrobial Properties of Graphene Oxide Nanosheets: Why Size Matters. *ACS Nano* **2015**, *9*, 7226−7236.
(32) Di Giulio, M.; Zappacosta, R.; Di Lodovico, S.; Di Campli, E.; Siani, G.; Fontana, A.; Cellini, L. Antimicrobial and Antibiofilm Efficacy of Graphene Oxide against Chronic Wound Microorganisms. *Antimicrob. Agents Chemother.* **2018**, *62*, e00547−18.
(33) Al-Jumaili, A.; Alancherry, S.; Bazaka, K.; Jacob, M. V. Review on the Antimicrobial Properties of Carbon Nanostructures. *Materials* **2017**, *10*, 1066.
(34) Han, D.; Yan, L.; Chen, W.; Li, W. Preparation of chitosan/graphene oxide composite film with enhanced mechanical strength in the wet state. *Carbohydr. Polym.* **2011**, *83*, 653−658.
(35) Pan, Y.; Wu, T.; Bao, H.; Li, L. Green fabrication of chitosan films reinforced with parallel aligned graphene oxide. *Carbohydr. Polym.* **2011**, *83*, 1908−1915.
(36) Chen, P.; Xie, F.; Tang, F.; McNally, T. Structure and properties of thermomechanically processed chitosan/carboxymethyl cellulose/graphene oxide polyelectrolyte complexed bionanocomposites. *Int. J. Biol. Macromol.* **2020**, *158*, 420−429.
(37) Yang, J.; Pruvost, S.; Livi, S.; Duchet-Rumeau, J. Understanding of Versatile and Tunable Nanostructuration of Ionic Liquids on Fluorinated Copolymer. *Macromolecules* **2015**, *48*, 4581−4590.
(38) Remsing, R. C.; Swatloski, R. P.; Rogers, R. D.; Moyna, G. Mechanism of cellulose dissolution in the ionic liquid 1-n-butyl-3-methylimidazolium chloride: A 13C and 35/37Cl NMR relaxation study on model systems. *Chem. Commun.* **2006**, *12*, 1271−1273.
(39) Mateyawa, S.; Xie, D. F.; Truss, R. W.; Halley, P. J.; Nicholson, T. M.; Shamshina, J. L.; Rogers, R. D.; Boehm, M. W.; McNally, T. Effect of the ionic liquid 1-ethyl-3-methylimidazolium acetate on the phase transition of starch: Dissolution or gelatinization? *Carbohydr. Polym.* **2013**, *94*, 520−530.
(40) Zhang, B.; Xie, F.; Shamshina, J. L.; Rogers, R. D.; McNally, T.; Halley, P. J.; Truss, R. W.; Chen, L.; Zhao, S. Dissolution of Starch with Aqueous Ionic Liquid under Ambient Conditions. *ACS Sustainable Chem. Eng.* **2017**, *5*, 3737−3741.
(41) Chen, P.; Xie, F.; Tang, F.; McNally, T. Structure and properties of thermomechanically processed silk peptide and nanoclay filled chitosan. *Nanocomposites* **2019**, Submitted.
(42) Layek, R. K.; Kundu, A.; Nandi, A. K. High-Performance Nanocomposites of Sodium Carboxymethylcellulose and Graphene Oxide. *Macromol. Mater. Eng.* **2013**, *298*, 1166−1175.
(43) Shahzadi, K.; Mohsin, I.; Wu, L.; Ge, X.; Jiang, Y.; Li, H.; Mu, X. Bio-Based Artificial Nacre with Excellent Mechanical and Barrier Properties Realized by a Facile In Situ Reduction and Cross-Linking Reaction. *ACS Nano* **2017**, *11*, 325−334.
(44) El Miri, N.; Abdelouahdi, K.; Barakat, A.; Zahouily, M.; Fihri, A.; Solhy, A.; El Achaby, M. Bio-nanocomposite films reinforced with cellulose nanocrystals: Rheology of film-forming solutions, transparency, water vapor barrier and tensile properties of films. *Carbohydr. Polym.* **2015**, *129*, 156−167.
(45) Rosca, C.; Popa, M. I.; Lisa, G.; Chitanu, G. C. Interaction of chitosan with natural or synthetic anionic polyelectrolytes. 1. The chitosan−carboxymethylcellulose complex. *Carbohydr. Polym.* **2005**, *62*, 35−41.
(46) Lawrie, G.; Keen, I.; Drew, B.; Chandler-Temple, A.; Rintoul, L.; Fredericks, P.; Grøndahl, L. Interactions between Alginate and

https://dx.doi.org/10.1021/acsomega.0c02418
ACS Omega XXXX, XXX, XXX−XXX

Chitosan Biopolymers Characterized Using FTIR and XPS. *Biomacromolecules* **2007**, *8*, 2533−2541.
(47) Pawlak, A.; Mucha, M. Thermogravimetric and FTIR studies of chitosan blends. *Thermochim. Acta* **2003**, *396*, 153−166.
(48) Chen, Z.; Mo, X.; He, C.; Wang, H. Intermolecular interactions in electrospun collagen−chitosan complex nanofibers. *Carbohydr. Polym.* **2008**, *72*, 410−418.
(49) Xie, D. F.; Martino, V. P.; Sangwan, P.; Way, C.; Cash, G. A.; Pollet, E.; Dean, K. M.; Halley, P. J.; Avérous, L. Elaboration and properties of plasticised chitosan-based exfoliated nano-biocomposites. *Polymer* **2013**, *54*, 3654−3662.
(50) Xie, F.; Luckman, P.; Milne, J.; McDonald, L.; Young, C.; Tu, C. Y.; Pasquale, T. D.; Faveere, R.; Halley, P. J. Thermoplastic starch: Current development and future trends. *J. Renewable Mater.* **2014**, *2*, 95−106.
(51) Martino, V.; Pollet, E.; Avérous, L. Novative biomaterials based on chitosan and poly(ε-caprolactone): Elaboration of porous structures. *J. Polym. Environ.* **2011**, *19*, 819−826.
(52) Wendler, F.; Todi, L.-N.; Meister, F. Thermostability of imidazolium ionic liquids as direct solvents for cellulose. *Thermochim. Acta* **2012**, *528*, 76−84.
(53) Singh, S.; Varanasi, P.; Singh, P.; Adams, P. D.; Auer, M.; Simmons, B. A. Understanding the impact of ionic liquid pretreatment on cellulose and lignin via thermochemical analysis. *Biomass Bioenergy* **2013**, *54*, 276−283.
(54) Chen, Q.; Xu, A.; Li, Z.; Wang, J.; Zhang, S. Influence of anionic structure on the dissolution of chitosan in 1-butyl-3-methylimidazolium-based ionic liquids. *Green Chem.* **2011**, *13*, 3446−3452.
(55) Stankovich, S.; Dikin, D. A.; Piner, R. D.; Kohlhaas, K. A.; Kleinhammes, A.; Jia, Y.; Wu, Y.; Nguyen, S. T.; Ruoff, R. S. Synthesis of graphene-based nanosheets via chemical reduction of exfoliated graphite oxide. *Carbon* **2007**, *45*, 1558−1565.
(56) Quijada-Garrido, I.; Laterza, B.; Mazón-Arechederra, J. M.; Barrales-Rienda, J. M. Characteristic Features of Chitosan/Glycerol Blends Dynamics. *Macromol. Chem. Phys.* **2006**, *207*, 1742−1751.
(57) Quijada-Garrido, I.; Iglesias-González, V.; Mazón-Arechederra, J. M.; Barrales-Rienda, J. M. The role played by the interactions of small molecules with chitosan and their transition temperatures. Glass-forming liquids: 1,2,3-Propantriol (glycerol). *Carbohydr. Polym.* **2007**, *68*, 173−186.
(58) Bonanos, N.; Steele, B. C. H.; Butler, E. P. Applications of Impedance Spectroscopy. In *Impedance Spectroscopy*; Barsoukov, E.; Macdonald, J. R., Eds.; John Wiley & Sons, Inc.: Hoboken, NJ, U.S.A., 2005; pp 205−537.
(59) Wang, X.; Chi, Y.; Mu, T. A review on the transport properties of ionic liquids. *J. Mol. Liq.* **2014**, *193*, 262−266.
(60) Osman, Z.; Ibrahim, Z. A.; Arof, A. K. Conductivity enhancement due to ion dissociation in plasticized chitosan based polymer electrolytes. *Carbohydr. Polym.* **2001**, *44*, 167−173.
(61) Khiar, A. S. A.; Puteh, R.; Arof, A. K. Conductivity studies of a chitosan-based polymer electrolyte. *Phys. B* **2006**, *373*, 23−27.
(62) Navaratnam, S.; Ramesh, K.; Ramesh, S.; Sanusi, A.; Basirun, W. J.; Arof, A. K. Transport mechanism studies of chitosan electrolyte systems. *Electrochim. Acta* **2015**, *175*, 68−73.
(63) Wang, Q.; Zhu, L. Polymer nanocomposites for electrical energy storage. *J. Polym. Sci., Part B: Polym. Phys.* **2011**, *49*, 1421−1429.
(64) Li, J.; Seok, S. I.; Chu, B.; Dogan, F.; Zhang, Q.; Wang, Q. Nanocomposites of Ferroelectric Polymers with TiO2 Nanoparticles Exhibiting Significantly Enhanced Electrical Energy Density. *Adv. Mater.* **2009**, *21*, 217−221.
(65) Barber, P.; Balasubramanian, S.; Anguchamy, Y.; Gong, S.; Wibowo, A.; Gao, H.; Ploehn, J. H.; Zur Loye, H.-C. Polymer Composite and Nanocomposite Dielectric Materials for Pulse Power Energy Storage. *Materials* **2009**, *2*, 1697−1733.
(66) Fadzallah, I. A.; Majid, S. R.; Careem, M. A.; Arof, A. K. Relaxation process in chitosan−oxalic acid solid polymer electrolytes. *Ionics* **2014**, *20*, 969−975.
(67) Bhatt, A. S.; Bhat, D. K.; Santosh, M. S.; Tai, C.-w. Chitosan/NiO nanocomposites: a potential new dielectric material. *J. Mater. Chem.* **2011**, *21*, 13490−13497.
(68) Bowen, C. R.; Buschhorn, S.; Adamaki, V. Manufacture and characterization of conductor-insulator composites based on carbon nanotubes and thermally reduced graphene oxide. *Pure Appl. Chem.* **2014**, *86*, 765−774.

https://dx.doi.org/10.1021/acsomega.0c02418
ACS Omega XXXX, XXX, XXX−XXX